Malaysian Journal of Chemistry, 2024, Vol. 26(5), 46-55
(Special Issue: *3rd Virtual International Symposium on Sciences 2023*)

Surface and Textural Analyses for Bimetallic Nickel-Based Catalyst onto Various Support using Microwave Assisted Synthesis

Salma Samidin[1], Azizul Hakim Lahuri[3], Wan Nor Roslam Wan Isahak[1,2]*, Khairul Naim Ahmad[1,2], Muhammad Rahimi Yusop[4] and Norliza Dzakaria[5,6]

[1]Department of Chemical and Process Engineering, Faculty of Engineering and Built Environment, Universiti Kebangsaan Malaysia, 43600 UKM Bangi, Selangor, Malaysia

[2]Research Centre for Sustainable Process Technology (CESPRO), Faculty of Engineering and Built Environment, Universiti Kebangsaan Malaysia, 43600 UKM Bangi, Selangor, Malaysia

[3]Department of Science and Technology, Universiti Putra Malaysia Bintulu Campus, Nyabau Road, P. O. Box 396, 97008 Bintulu, Sarawak, Malaysia

[4]Department of Chemical Sciences, Faculty of Science and Technology, Universiti Kebangsaan Malaysia, 43600 UKM Bangi, Selangor, Malaysia

[5]School of Chemistry and Environment, Faculty of Applied Science, Universiti Teknologi Mara (UiTM) Cawangan Negeri Sembilan, Kampus Kuala Pilah, 72000 Kuala Pilah, Negeri Sembilan, Malaysia

[6]Advanced Material for Environmental Remediation (AMER) Research Group, Faculty of Applied Science, Universiti Teknologi Mara (UiTM) Cawangan Negeri Sembilan, Kampus Kuala Pilah, 72000 Kuala Pilah, Negeri Sembilan, Malaysia

*****Corresponding author (e-mail: wannorroslam@ukm.edu.my)

The synthesis of a bimetallic nickel catalyst via the integration of different support materials comprising Al_2O_3, SiO_2, and dolomite was analysed and compared. The catalysts were synthesised using a microwave monomode reactor for 11 minutes at a temperature of 160 °C. The primary characterisation methods utilised for the investigation of reduction behaviour were temperature-programmed reduction (TPR), X-ray diffraction, and N_2 adsorption-desorption isotherm. The original structure of oxides Ni and Cr-Ni can be altered using silicon dioxide (SiO_2), aluminium oxide (Al_2O_3), and dolomite ($CaMg(CO_3)_2$), which have all been subjected to research, indicating that there is a significant interaction between the catalyst and support. After the addition of the support, the distribution determined using Barrett-Joyner-Halenda (BJH) calculations indicates a broad pore size range that encompasses both meso (2-50 nm) and macro pore (>50 nm). In comparison to catalysts alone, oxides of Ni and Cr-Ni that contain SiO_2 have a greater surface area. Whereas SiO_2 was found to effectively enhance the surface area of oxide Ni compared to Al_2O_3 and dolomite as supporting materials. The utilisation of SiO_2 on the Ni-based catalysts caused the temperature of the TPR peak to decrease to 392 °C, compared to Al_2O_3 and dolomite. This may be attributed to two factors: weak interaction on SiO_2, the surface area, and porosity thus leading to easier diffusion of gas reductant, and accessibility of reactants during reduction thus enhancing the reduction of NiO species.

Keywords: Reduction behaviour; support catalyst; nickel oxide; bimetallic catalysts

Received: October 2023; Accepted: February 2024

Significant modifications have been made in catalysis for renewable energy production, sensing, and electronics in the past decades due to developments in material science and engineering. Altering the properties of catalysts by changing their structure and composition provides researchers with the tools they need to better understand the fundamental properties of materials such as new spectroscopic, microscopic, and nanofabrication techniques [1]. This greatly improves multicomponent commercial catalysts in the field of catalysis.

Choosing a suitable support may be crucial for the catalyst's performance since it may imply a poor or strong metal-support interaction that affects the adsorption ability and catalytic features [2]. Al_2O_3-based support is often used in chemical reactions such as reforming due to its mechanical and chemical resistance [3]. Meanwhile, other support modifiers such as ZrO_2, SiO_2, MgO, La_2O_3, CeO_2, and TiO_2 also have been utilised, with the catalysts showing enhanced conversion, higher redox properties, high thermal stability, and resistance to sintering due to their favourable properties [2, 4, 5]. In addition to CaO, which is a naturally occurring metal oxide that is present around the planet, magnesium oxide (MgO) has also been thought of as an additive because it can be found in dolomite [6]. Due to its catalytic tar

†Paper presented at the 3rd Virtual International Symposium on Sciences (3rd VISoS 2023)

cracking and anti-sintering qualities, dolomite, a naturally occurring mineral of which primary component is $CaMg(CO_3)_2$, is desirable as a non-toxic base catalyst and CO_2 sorbent in thermochemical conversion processes such as biofuels [7].

Several catalyst preparation methods can be applied to obtain well-distributed active metal on support material that showed a significant impact on the catalyst's performance, such as impregnation, co-precipitation, sol-gel technique [8]. The impregnation is mostly utilised by researchers as it is the simplest approach for catalyst synthesis. However, the conventional wet impregnation method requires long hours of stirring [9–11] to achieve good dispersion of the catalyst on the support materials [12]. Besides that, a set temperature during stirring results in a low heating rate; the stirring condition also leads to greater heat loss. These phenomena can be prevented by adopting the microwave-assisted technique. One study used the microwave-assisted technique for developing bimetallic catalysts, proving their potential in providing homogenous internal and volumetric heating at high rates within a short time [13]. The radiation generated by microwave can provide better homogeneous heating, resulting in the nucleation of small particles to obtain nanoparticles [14]. Furthermore, it has been demonstrated that microwave procedures are more energy-efficient and environmentally benign than conventional processes, and that they have been effectively employed in both organic and inorganic syntheses [15]. Therefore, this work attempts to adopt microwave-assisted synthesis in catalyst preparation.

Active metals of nickel-based catalysts are widely recognised as commercial catalysts due to their low cost, ubiquitous availability, and excellent catalytic characteristics. However, due to metal agglomeration and carbon production, they are prone to deactivation. Previously, we had reported the chemical behaviour of mono and bimetallic Ni-based nanocatalyst via temperature programmed reduction (TPR) study [16, 17]. By suitably introducing support to the catalyst's surface, a catalytic synergistic effect between the active phases and the support may be achieved, increasing the reducibility of Ni and preventing sintering. Hence, in this work, we used microwave-assisted synthesis techniques to add support systems to the mono and bimetallic Ni-based catalysts. The synthesised catalysts were examined using powder X-ray diffraction (XRD), Brunauer-Emmett-Teller (BET) for surface area measurements, and temperature-programmed reduction (TPR). The effect of incorporating various support would be subsequently discussed.

EXPERIMENTAL

Sample Preparation

Mono and bi-metallic Ni-based with supported catalysts were prepared by microwave-assisted synthesis using commercial SiO_2, Al_2O_3, and dolomite support with $Ni(NO_3)_2.6H_2O$ and $CrN_3O_9{\cdot}9H_2O$ solutions, respectively. For microwave-assisted synthesis, nitrate precursors of Ni and Cr with 10% wt. (ratios 1:9) and SiO_2, Al_2O_3, and dolomite were placed in a sample tube containing 5 mL of ethanol liquid. The deionised water was measured using a new sample tube approximately half of the sample tube. Then, the deionised water was added to the mixture. The mixture was centrifuged at 600 rpm for 11 minutes at a temperature of 160 °C using a monomode microwave reactor. The mixture was dried in an oven overnight at 120 °C and the catalysts were ground to obtain a powder texture. Finally, it was calcined using a furnace at a temperature of 400 °C for 4 hours. All the prepared samples are denoted as NiO/SiO_2, NiO/Al_2O_3, NiO/Dolomite and $CrNiO/SiO_2$, $CrNiO/Al_2O_3$, and CrNiO/Dolomite.

Characterisation Methods

The BET surface area and pore size distribution of the catalysts were obtained using a Micromeritics Tristar unit analyser with liquid nitrogen at 77.4 K as the adsorbate required for profiling the adsorption and desorption isotherms. A Bruker XRD-6000 diffractometer with Cu target K-α radiation source (40 kV, 30 mA) was used to analyse the crystalline phases of Ni0 and NiO in the sample. A scanning speed of 2° min^{-1} was used over an angular range of $20° < 2\theta < 80°$ for the XRD characterisation. The estimation of the average Ni crystallite size of the catalysts was carried out upon calcination of fresh catalysts in an air atmosphere at 700 °C for 4 hours. A scanning speed of 0.2° min^{-1} was used for 2θ range between 40-50° and Scherrer's equation was used for the estimation of the NiO/Ni^0 crystallite sizes.

The reducibility profiles of the catalysts were obtained from a CO-Temperature Programmed Reduction (CO-TPR) analysis which was conducted using an Autochem II Plus equipped with a thermal conductivity detector connected to a moisture trap. About 20 mL min^{-1} of 40% CO/N_2 probe gas mixture was passed through ~50 mg of sample which was heated from ambient conditions to 900 °C at a ramping rate of 10 °C min^{-1} to obtain the TPR profile.

RESULTS AND DISCUSSION

Catalysts Characterisation

Surface Study via N_2 Ad-desorption Analysis

Figures 1a, 1b, and 1c show the isotherm curve for N_2 ad-desorption whereas Figure 1ai-bi-ci indicates the pore size distribution of the prepared catalysts. The surface area value, volume, and pore size calculated using the BJH method for as-prepared catalysts with fresh support materials and fresh catalysts are summarised in Table 1. The SiO_2 curve in Figure 1a is classified as typical of type IV with the hysteresis loop

type H1 which indicates the capillary condensation effect that proves the existence of meso-pore composed of a uniform meso-pore range diameter [18, 19]. Type H1 is also classified with porous material consisting of agglomerate or compact uniform spherical arrangement with a narrow pore size distribution, in agreement with Figure 1ai [20]. Meanwhile, for Al_2O_3 (Figure 1b) and dolomite (Figure 1c), the isotherms curve is typical of type III with loop H3 exhibiting a porous existence or consisting of macro-pores, plate-like rigid aggregates, and a network of pores comprising macro-pores that are not completely filled with burrow condensation [19]. Furthermore, the Al_2O_3 and Dolomite samples are composed of a combination of meso and macro pores, in agreement with Figure 1bi and ci. As reported in the catalyst study, mesopore structure can provide good benefits and resistance to Ni sintering [21].

After the addition of a support system (SiO_2) into the mono and bimetallic catalysts, the isotherms remain and are classified as type IV with loop H1 which implies the formation of high mesopore [22]. Meanwhile, catalysts with Al_2O_3 supporter show typical physical adsorption of type IV but with the shape of a hysteresis loop H3. Occasionally, 10CrNiO-dolomite shows type V properties except for 10Ni-Dolomite (Figure 1c) which exhibits the properties of type III, indicating the presence of micropore structures. All samples exhibit a loop shape, indicating the presence of a mesopore structure [23]. This is in contrast to the fresh NiO and Cr-Ni without support which show typical properties of type III and typical IV hysteresis loop H3 (not shown here). This suggests that the presence of SiO_2 and dolomite materials on the mono and bimetallic catalysts completely dominates the initial catalyst structure except for Al_2O_3.

SiO_2 material shows a high surface area of 115.00 $m^2 g^{-1}$, compared to Al_2O_3 and Dolomite with values of 0.66 and 0.81 $m^2 g^{-1}$, respectively. The surface area of Al_2O_3 exhibits α-Al_2O_3 properties with a low surface area or better known as α-Al_2O_3 (<10 $m^2 g^{-1}$) [24]. It is well known that the surface area of α-Al_2O_3 is lower than that of γ-Al_2O_3 [25]. Alumina can exist in various phases such as Alpha (α) and Gamma (γ)-alumina phases. Indeed, α-Al_2O_3 has thermodynamic stability and some properties such as thermal stability, "*high hardness*", and stability of chemical properties. Meanwhile, the γ-Al_2O_3 is an unstable phase as it can easily switch phases at a low temperature of 600-700 °C and requires a high temperature of 950 °C for phase conversion to α-Al_2O_3 [26].

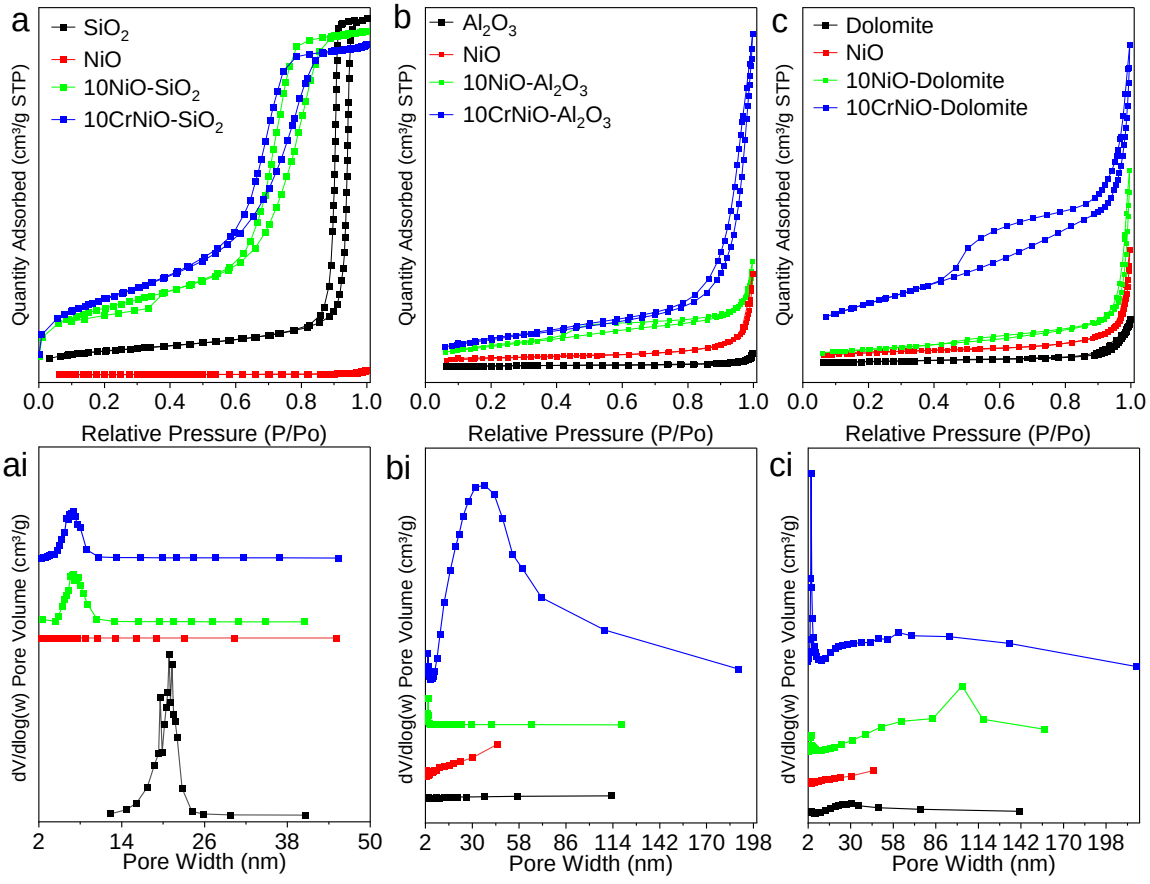

Figure 1. (a, b, c) N_2 adsorption-desorption analysis and (ai, bi, ci) BJH pore size distribution plots as-prepared catalysts.

Table 1. BET surface area, pore volume, and average pore width as-prepared catalysts calculated from **Figure 1** and **Figure 2.**

Catalysts	Surface Area (m^2/g)[a]	average pore width (nm)[b]	Pore Volume (cm^3/g)[b]	Crystallite size (nm)[c]
NiO	2.63	17.30	0.004	38.90
SiO_2	115.00	19.77	0.744	48.80
Al_2O_3	0.66	13.11	0.001	78.80
Dolomite	0.81	17.45	0.002	1.00
10NiO-SiO_2	323.00	6.46	0.717	12.20
10CrNiO-SiO_2	371.00	6.43	0.687	7.00
10NiO-Al_2O_3	5.90	6.53	0.007	19.00
10CrNiO-Al_2O_3	7.62	19.27	0.023	27.00
10NiO-Dolomite	3.37	19.47	0.006	21.50
10CrNiO-Dolomite	13.25	7.36	0.018	10.20

[a]BET
[b]BJH
[c]Scherrer equation XRD

The structural properties of supported Ni and Cr-Ni oxide with the addition of support materials as shown in Table 1 demonstrates that the catalyst series with SiO_2 has a high surface area with a range of 323.00-371.00 $m^2\ g^{-1}$ compared to α-Al_2O_3 supported catalysts (5.90-7.62 $m^2\ g^{-1}$) and dolomite (3.37-13.25 $m^2\ g^{-1}$). The presence of SiO_2 increases the surface area of Ni and Cr-Ni oxide catalysts compared to unsupported ones. However, it can be seen that the increase in surface area of the Ni oxide catalyst is only effective by using SiO_2 compared to Al_2O_3 and dolomite. The increase in catalyst surface area can be attributed to the formation of new external pores on the surface of NiO and the existence of mesopore formed after the addition of SiO_2 support, which then forms a new layer on the external surface of the catalyst [27]. The use of SiO_2 material can increase the porosity of the catalyst and can form a network of interconnected pores in the Ni matrix [28]. In addition, it has been proven that the addition of SiO_2 can help spread Ni particles more uniformly and prevent agglomeration as evidenced by the small crystal size (Table 1). In general, the formation of small crystal sizes will lead to an increase in the surface area of the catalyst after calcination [29].

Figure **2** shows an analysis of XRD diffractogram phase changes prior to the addition of a supporting system into the mono- and bi-metallic metal based on Ni catalysts. Generally, by comparing the mono and bimetal supported catalysts with NiO alone, the surface area for the catalysts supported is inversely proportional to the NiO crystallite size. The crystallite size for fresh NiO and supported were measured using a lattice plan with the highest intense peak at [200], [102], [113], and [006], respectively. The peaks that appear at 2θ:37.3°, 43.3°, 62.9°, 75.4°, and 79.7° can be attributed to the existence of the NiO phase (ICDD 01-078-0643) while the wide peak at an angle of ~22° can be described as the SiO_2 phase (ICDD 00-033-1161). The peak intensity increases for 10NiO-SiO_2 and there is a slight displacement of the 2θ angle of the NiO phase to a higher position which indicates a small contraction in the unit cell parameters during the catalyst preparation [30]. This is because nickel crystals have entered the SiO_2 pores and in turn change the lattice of the SiO_2 structure [31]. A lower intensity is observed at 2θ:22° for 10NiO-SiO_2 compared to 10CrNiO-SiO_2, which shows that the SiO_2 crystal structure is disturbed due to the incorporation of Ni ions into the lattice structure of the supports, leading to a decrease in crystal coherence. Furthermore, for bimetallic catalysts, the XRD spectrum showed a wide SiO_2 signal peak at 2θ:~22° with low/weak NiO crystal peaks visible at lattice plane positions [111], [200], and [220] and a new appearance peak at 2θ: 34.7°, which correspond to $NiCrO_4$ (ICDD 01-073-1046). This reveals that the addition of a second metal altered the electronic structure of the Ni species into a nano size. Table 1 shows that the addition of Cr decreased the crystal size of the Ni species (7.0 nm) compared to 10NiO-SiO_2 (12.2 nm). The decrease in crystal size may result from the addition of Cr and Ni, which can cause changes in crystal structure or growth mechanism with SiO_2 material. The presence of a second metal can lead to the formation of different phases of crystals or changes in the nucleation and growth rate of the crystals, which will affect the size of the final crystal after calcination. This is significant with the decrease in crystallite size of the Ni species in the CrNiO-SiO_2 sample. The nickel oxide phase is located in the meso pores and this is in line with the XRD patterns (Figure 2a), which shows the high intensity of the Ni oxide species (large crystal size) of sample NiO-SiO_2. The high intensity peaks of NiO-SiO_2 are also due to

the concentrated dispersion of X-rays to the highly crystalline NiO species versus SiO_2 which in turn produces low SiO_2 intensity peaks on the XRD diffractograms [32]. As a result, Ni species particles scattered well above SiO_2 after going through the drying process upon the addition of the Cr promoter [33], which is in agreement with the increase in surface area as shown in Table 1. Figure 2b shows that Al_2O_3 peaks are present at positions 2θ: 25.7, 35.2, 37.9, 43.4, 52.6, 57.6, 61.4, 66.7, 68.3, and 77.1° with ICDD reference numbers 00-010-0173, respectively [26]. Meanwhile, the angle at position 2θ: 37.4°, 43.4°, 63.0°, 75.7°, and 79.6° with lattice [111], [200], [220], [311], and [222] corresponds to the NiO species (ICDD 01-078-0643) while a new peak crystal at 2θ: 35.9° corresponds to the formation of alloy $NiCrO_4$ with ICDD 00-073-1046. The crystal size of NiO is certainly measured based on the highest peak angled at 2θ: 43.4°. However, the peak is overlapped with the peak of NiO and Al_2O_3; therefore, it is likely that the oxide phases of Ni and Al have formed a new species of $NiAl_2O_4$ at peaks 2θ: 37°, 42° and 63° (ICDD 00-001-1299), which is in agreement with previous research [2]. Thus, the crystallite size for Ni species for the prepared catalyst supported with Al_2O_3 is determined by reference to the lattice plane of nickel oxide [111] at an angle of 2θ: 37.3°. The addition of Al_2O_3 support increases the size of the nickel crystals compared to catalysts supported by SiO_2 (Table 1).

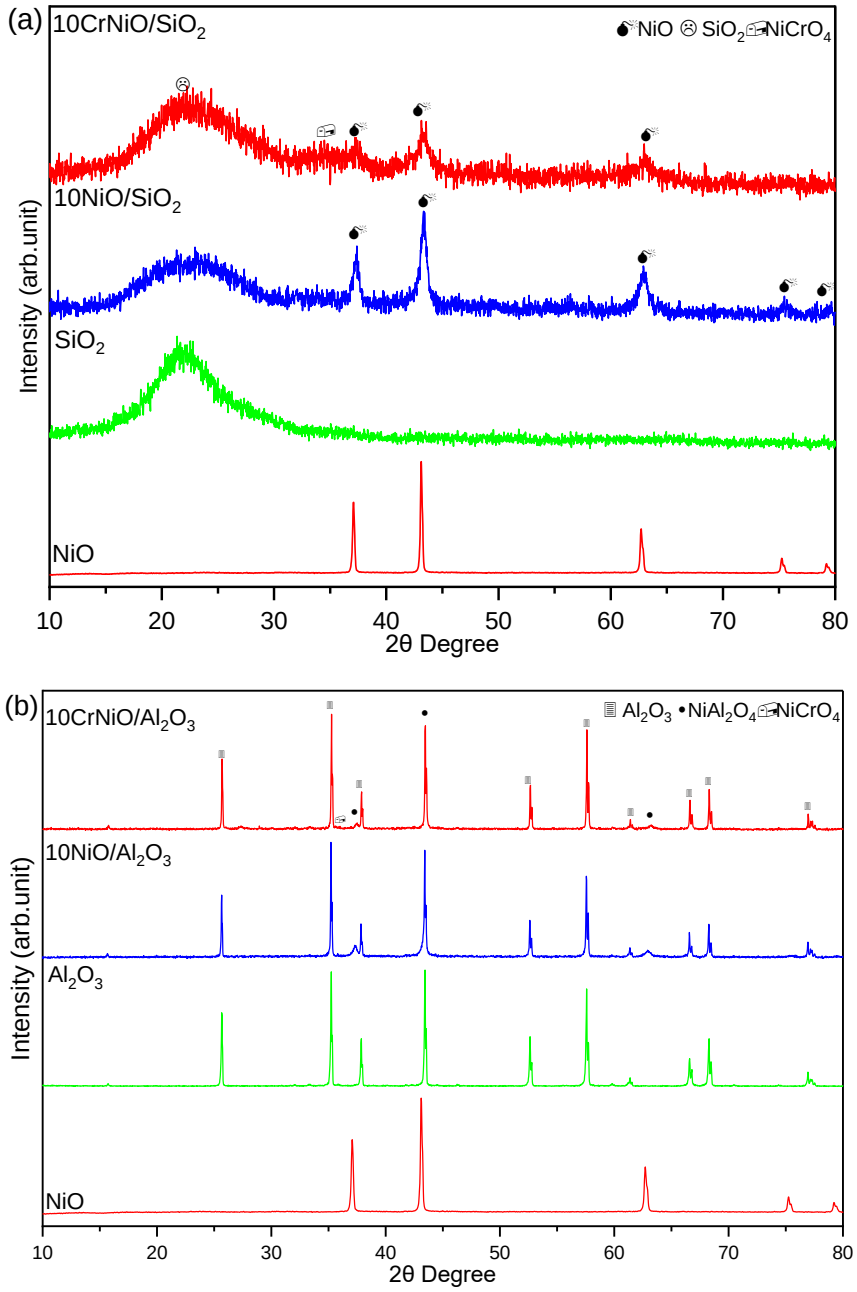

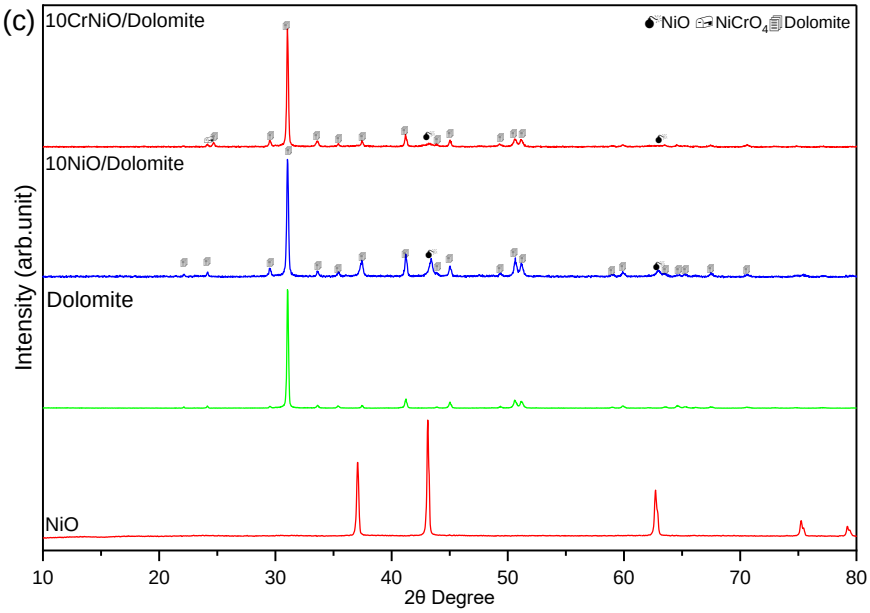

Figure 2. XRD diffractogram of mono- and bi-metallic Ni-based catalyst supported by (a) SiO_2, (b) Al_2O_3, and (c) Dolomite.

By comparing the catalysts supported by Al_2O_3 with catalysts supported by SiO_2, the surface area of catalysts supported by Al_2O_3 is inversely proportional to the crystallite size of the NiO. This might correspond to the addition of a metallic charge to Al_2O_3 which causes particles to form during solid drying, limited to producing new pores. Figure 2c shows the presence of dolomite ($CaMg(CO_3)_2$) phase peaks at position 2θ: 22.1-75.4° (ICDD 00-075-1711). The addition of dolomite into mono- and bi-metal oxide shows the decrease in crystal size for the Ni species (Table 1). The addition of Cr shows an alloy peak at 2θ:24.5°, which corresponds to $NiCrO_4$ (ICDD 00-021-0596). Overall, the XRD study shows the decrease in crystal size for the NiO species in mono- and bi-metallic for all the prepared catalysts compared to unsupported NiO. The formation of small crystallite is due to the interaction between NiO and support materials (nucleation sites) which alter and inhibit the growth of larger crystallite [34].

Reducibility Study

Temperature Programmed Reduction (TPR), as shown in Figure 3, was used to examine the reducibility of oxide species and their interactions with various support systems. We conducted a comparative analysis using unsupported mono- and bi-metallic Ni-based catalysts, referring to our previous studies, to understand the effect of various support systems on NiO reduction [17]. Three steps of NiO reduction stages I, II, and III were recorded at the temperature range of 400-700 °C [16]. Different NiO species were found in SiO_2, Al_2O_3, and dolomite when the TPR curve was deconvolved and fitted. Figure 3a shows four different reduction peaks. The initial and second peaks for NiO-SiO_2, NiO-Al_2O_3, and NiO-Dolomite took place at 392, 404, and 478 °C (red line) and 436, 460 and 539 °C (green line), indicating the partial reduction of NiO species at surface while Bourdouard reaction ($2CO\ (g) \rightarrow CO_2\ (g) + C\ (s)$) occurred during the reduction process which in agreement with a previous study [35]. According to earlier studies [24, 36], this peak represents a reduction of weakly-attached NiO with relatively limited dispersion on the support system. It is interesting to note that the dolomite support induced a rise in the NiO reduction temperature to 478 and 539 °C, which may be the result of a moderate interaction between bulk oxide species on the dolomite crystal surface [21]. Convolution peaks also occurred at 506 °C (NiO-SiO_2), 502 °C (NiO-Al_2O_3), and 645 °C (NiO-dolomite) (blue line) and at 584 °C (NiO-SiO_2), 730 °C (NiO-Al_2O_3), and 790 °C (NiO-dolomite) (pink line), which are related to the reduction of spinel type NiO species and solid solution (i.e NiO-CaO, NiO-MgO). It is noteworthy that the peak region of the pink curve (NiO-SiO_2) shows a high concentration of NiO actively interacting with SiO_2. According to this pattern, SiO_2 increased the reducibility of NiO species, probably as a result of better metal dispersion, as corroborated by the XRD diffractogram data (Figure 2a). The well-dispersed NiO particles may have formed more easily due to SiO_2's greater surface area, increasing the amount of active sites available for reduction [37].

With regards to bimetallic CrNi oxide, Figure 3b illustrates its reducibility behaviour as supported by SiO_2, Al_2O_3, and dolomite. Shoulder peaks at 203, 268, and 345 °C for CrNiO-SiO_2, CrNiO-Al_2O_3, and CrNiO-Dolomite, respectively, are associated with the surface-level conversion of Cr^{6+} to Cr^{3+} [17]. Contrary to the supported monometallic, the addition of support systems into the bimetallic catalyst led to a shift

towards lower temperatures. This change may be attributable to the synergistic actions of Cr and Ni, which improve the overall reducibility qualities. It is interesting to note that the CrNiO-Al_2O_3 curve (blue line) showed a broad and intense peak, indicating higher CO dissociation at 531 °C. This result suggests a larger concentration of species that can be reduced and effectively reduced [19]. Three different Ni species (α, β, γ) have been discovered in NiO/Al_2O_3 catalysts in earlier investigations. The α-type species have poor metal-support interactions and are active at low temperatures, whereas the β-type interacts more strongly with the support and promotes region reduced at moderate temperatures. $NiAl_2O_4$, which represents the γ-type, can only be reduced at high temperatures (750–900 °C) [21]. The expansion of the TPR peak for Ni and Cr-NiO/dolomite between 500 and 600 °C may be due to the coexistence of two reduction stages: homogenous NiO-MgO solid solution and free-state NiO (poor contact with support) [38]. As the temperature rises, the peak gradually goes down, indicating that there is a uniform NiO-MgO solid solution, which is one of the hardest phases to reduce. Dolomite introduces a number of oxide-support metal interaction phases, including solid solutions (NiO-MgO) and spinel NiO ($NiCr_2O_4$), which are difficult to distinguish [21]. Compared to SiO_2 and Al_2O_3, the NiO reduction for CrNiO/dolomite was more evident at higher temperatures for stage I, as previously reported [39]. The reduction temperature further shifted to 629 °C with three overlap deconvulated peaks at 345, 492, and 602 °C due to the interaction between Ni and the components of dolomite, which creates the stable nickel phase $NiMgO_2$ [40]. Meanwhile, stage II for NiO located at 645 and 790 °C and Cr-Ni samples at 776, 689, 808, and 845 °C indicated the reduction of strongly bound Ni^{2+} ions

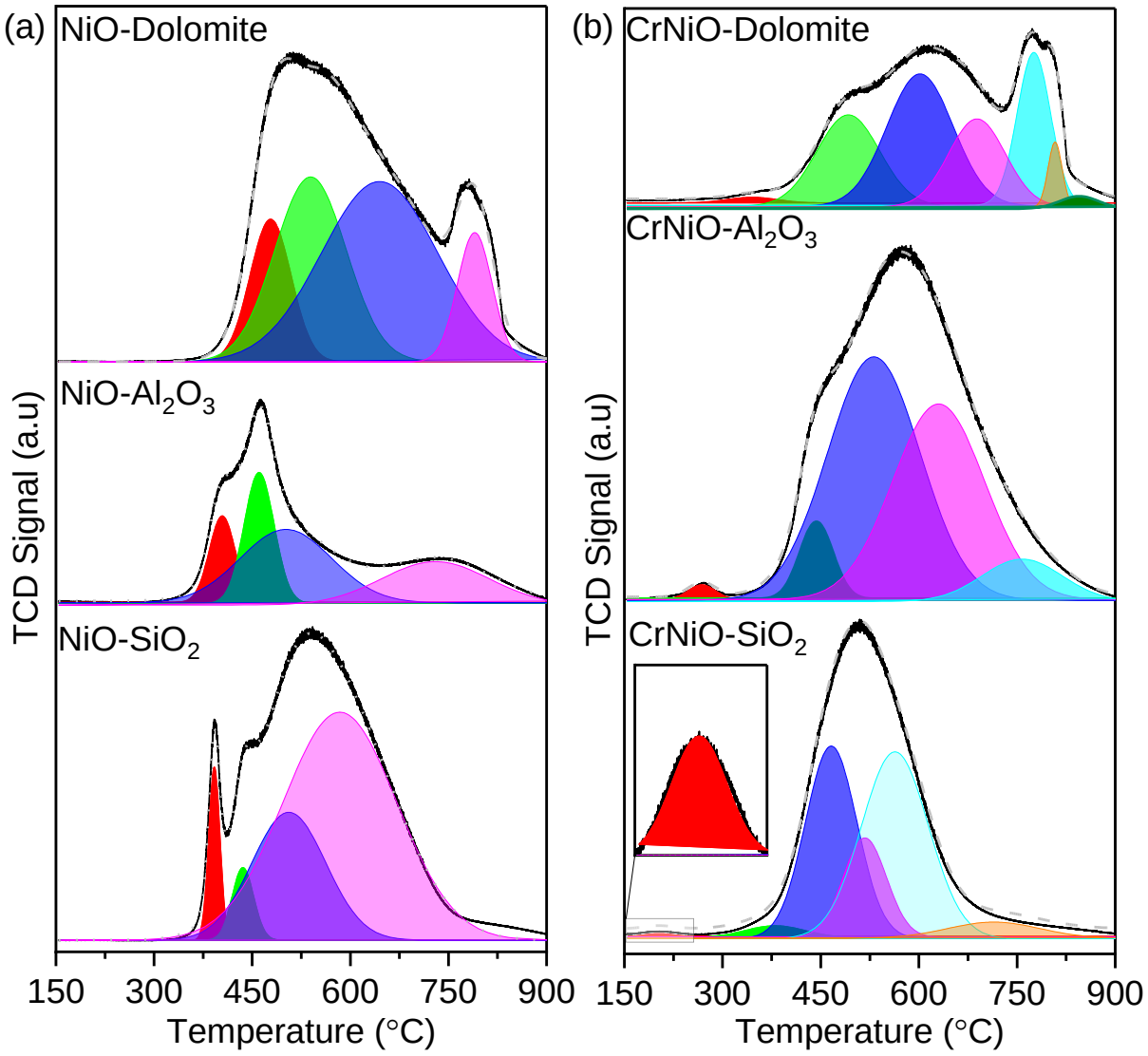

Figure 3. The deconvolution integration curve of TPR profile for (a) mono- and (b) bi-metallic Ni-based catalysts supported by SiO_2, Al_2O_3, and Dolomite

and oxide clusters inside the dolomite pores [41, 42]. Stage II for metal oxide supported by SiO_2 corresponds to NiO reduction with significant interaction with SiO_2 [39]. Additionally, the existence of crystals within the supporting pores, which is a result of the metal extraction process during calcination, may be responsible for the broad peak of CrNiO-Al_2O_3 reaching close to 900 °C [43]. This finding is consistent with the BET analysis, which shows that CrNiO-Al_2O_3 has greater pore volume and diameter.

CONCLUSION

The TPR results shed light on the reducibility behaviour of NiO and bimetallic CrNi oxide supported by SiO_2, Al_2O_3, and dolomite. The reduction characteristics and active species interactions are heavily influenced by the support materials. It is noteworthy that the CrNiO-SiO_2 exhibited the lowest reduction temperature at 392 °C compared to CrNiO-Al_2O_3 and CrNiO-Dolomite due to weak interaction between CrNiO and SiO_2. The findings are critical for catalyst design and optimisation, allowing for application-specific catalytic performance. Future studies might look into enhanced characterisation techniques to better understand the relationships and processes behind the observed patterns.

ACKNOWLEDGEMENTS

Authors are deeply grateful to Universiti Kebangsaan Malaysia (UKM) for their generous support of this project through the research grant code DIP-2022-010. They also extend their sincere thanks to Universiti Pertanian Malaysia (UPM) for their invaluable contribution through research grant 6300940-OCIM Sdn. Bhd. Furthermore, the authors would like to express their appreciation to the i-CRIM Laboratory at ALAF-UKM for their outstanding analytical services, which significantly enhanced the quality of this work.

REFERENCES

1. Monai, M., Melchionna, M. and Fornasiero, P. (2018) Chapter One - From metal to metal-free catalysts: Routes to sustainable chemistry. *Advances in Catalysis*, **63**, 1–73.

2. Moghaddam, S. V., Rezaei, M., Meshkani, F. and Daroughegi R. (2018) Synthesis of nanocrystalline mesoporous Ni/Al_2O_3–SiO_2 catalysts for CO_2 methanation reaction. *International Journal of Hydrogen Energy*, **43**, 19038–19046.

3. Ochoa, A., Bilbao, J., Gayubo, A. G. and Castaño, P. (2020) Coke formation and deactivation during catalytic reforming of biomass and waste pyrolysis products: A review. *Renewable and Sustainable Energy Reviews*, **119**, 109600.

4. Abate, S., Mebrahtu, C., Giglio, E., Deorsola, F., Bensaid, S., Perathoner, S., Pirone, R. and Centi, G. (2016) catalytic performance of γ-Al_2O_3-ZrO_2-TiO_2-CeO_2 composite oxide supported Ni-based catalysts for CO_2 methanation. *Industrial & Engineering Chemistry Research*, **55**, 4451–4460.

5. Kathiraser, Y., Wang, Z., Ang, M. L., Mo, L., Li, Z., Oemar, U. and Kawi, S. (2017) Highly active and coke resistant Ni/SiO_2 catalysts for oxidative reforming of model biogas: Effect of low ceria loading. *Journal of CO2 Utilization*, **19**, 284–295.

6. Sunphorka, S., Poonsritanakul, O. and Kuchonthara, P. (2019) Chemical-looping combustion of methane using $CaSO_4$ as an oxygen carrier: Effects of MgO addition. *Arabian Journal for Science and Engineering*, **44**, 5359–5370.

7. Xu, T., Xiao, B., Gladson, Moyo, G., Li, F., Chen, Z., Wang, X., Hu, Z., Liu, S. and Hu, M. (2019) Syngas production via chemical looping reforming biomass pyrolysis oil using NiO/dolomite as oxygen carrier, catalyst or sorbent. *Energy Conversion and Management*, **198**, 111835.

8. Sivakumar, V., Mohamed, A. R., Abdullah, A. Z. and Chai, S. P. (2010) Role of reaction and factors of carbon nanotubes growth in chemical vapour decomposition process using Methane-A highlight. *Journal of Nanomaterials*, *2010*, 1–11.

9. Lahuri, A. H., and Yarmo M. A. (2022) Study of CO_2 Adsorption time for carbonate species and linear CO_2 formations onto bimetallic CaO/Fe_2O_3 by Infrared Spectroscopy. *Sains Malaysiana*, **51**, 507-17.

10. Lahuri, A. H., Rahim, A. A., Nordin, N., Adnan, R., Jaafar, N. F. and Taufiq-Yap, Y. H. (2023) Comparative studies on adsorption isotherm and kinetic for CO_2 capture using iron oxide impregnated activated carbon. *Catalysis Today*, **418**, 114111.

11. Lahuri, A. H., Yarmo, M. A., Dzakaria, N., Ramlan, N. S. H., and Samidin, S. (2024) Temperature programmed desorption of carbon dioxide on activated carbon supported bimetallic oxides of Ni-Fe. *AIP Conference Proceedings*, **2925**.

12. Lahuri, A. H., Yusuf, A. M., Adnan, R., Rahim, A. A., Waheed Tajudeen, N. F. and Nordin, N. (0000) Kinetics and thermodynamic modeling for CO_2 capture using NiO supported activated carbon by temperature swing adsorption. *Bio interface Research in Applied Chemistry*, **12**, 4200–19.

13. Shakir, M., Kushwaha, S. K., Maurya, K. K., Bhagavannarayana, G. and Wahab, M. A. (2009) Characterization of ZnSe nanoparticles synthesized

by microwave heating process. *Solid State Communications*, **149**, 2047–2049.

14. Jaimes-paez, C. D., Vences-alvarez, E., Salinas-torres, D. and Morall, E. (2023) Microwave-assisted synthesis of carbon-supported Pt nano-particles for their use as electrocatalysts in the oxygen reduction reaction and hydrogen evolution reaction. *Electrochimica Acta*, **464**, 142871.

15. Pang, M., Ding, L., Li, C. and Liang, C. (2010) Microwave-assisted preparation of Mo_2C/CNTs nanocomposites as efficient electrocatalyst supports for oxygen reduction reaction. *Industrial & Engineering Chemistry Research*, **49**, 4169–4174.

16. Samidin, S., Ahmad, K. N., Shamsuddin, M. R., Tahari, M. N. A., Lahuri, A. H., Salleh, F., Asikin Mijan, N., Jamil, M. S. M., Isahak, W. N. R. W., Yarmo, M. A. and Yusop, M. R. (2023) Role of Cr-doped NiO in reduction under a low concentration of H_2 and CO. *Surfaces and Interfaces*, **41**, 103106.

17. Liang, W., Yan, H., Chen, C., Lin, D., Tan, K., Feng, X., Liu, Y., Chen, X., Yang, C. and Shan, H. (2020) Revealing the effect of nickel particle size on carbon formation type in the methane decomposition reaction. *Catalysts*, **10**, 890.

18. Thommes, M., Kaneko, K., Neimark, A. V., Olivier, J. P., Rodriguez-Reinoso, F., Rouquerol, J. and Sing, K. S. W. (2015) Physisorption of gases, with special reference to the evaluation of surface area and pore size distribution (IUPAC Technical Report). *Pure and Applied Chemistry*, **87**, 1051–1069.

19. Blanco, P. H., Wu, C. and Williams, P. T. (2014) Influence of Ni/SiO_2 catalyst preparation methods on hydrogen production from the pyrolysis/ reforming of refuse derived fuel. *International Journal of Hydrogen Energy*, **39**, 5723–5732.

20. Tan, R. S., Tuan Abdullah, T. A., Mahmud, S. A., Md Zin, R. and Md Isa, K. (2019) Catalytic steam reforming of complex gasified biomass tar model toward hydrogen over dolomite promoted nickel catalysts. *International Journal of Hydrogen Energy*, **44**, 21303–21314.

21. Xiao, Y. -L., Ding, M. -J., Wang, R. -J., Sun, H. -L., Zhang, J. -G., Pan, Q. -J. and Guo, Y. -R. (2019) Fabrication of mesoporous SiO_2@SLS composite to remove organic pollutants: hydrogen bond-induced intriguing changes of solubility. *Journal of Nanoparticle Research*, **21**, 18.

22. Belhachemi, M., Belala, Z., Lahcene, D. and Addoun, F. (2009) Adsorption of phenol and dye from aqueous solution using chemically modified date pits activated carbons. *Desalination and Water Treatment*, **7**, 182–190.

23. Alberton, A. L., Souza, M. M. V. M. and Schmal, M. (2007) Carbon formation and its influence on ethanol steam reforming over Ni/Al_2O_3 catalysts. *Catalysis Today*, **123**, 257–264.

24. He, L., Hu, S., Jiang, L., Liao, G., Chen, X., Han, H., Xiao, L., Ren, Q., Wang, Y., Su, S. and Xiang, J. (2018) Carbon nanotubes formation and its influence on steam reforming of toluene over Ni/Al_2O_3 catalysts: Roles of catalyst supports. *Fuel Processing Technology*, **176**, 7–14.

25. Mohammed, A. A., Khodair, Z. T. and Khadom, A. A. (2020) Preparation and investigation of the structural properties of α-Al_2O_3 nanoparticles using the sol-gel method. *Chemical Data Collections*, **29**, 100531.

26. Dzakaria, N., Abu Tahari, M. N., Salleh, F., Samsuri, A., Azizi, M. A. H., Tengku Saharuddin, T. S., Yusop, M. R., Wan Isahak, W. N. R., Mohamed Hisham, M. W. and Yarmo, M. A. (2019) Chemical Reduction Behavior of Zirconia Doped to Nickel at Different Temperature in Carbon Monoxide Atmosphere. *Indonesian Journal of Chemistry*, **20**, 105.

27. Blanco, P. H., Wu, C., Onwudili, J. A. and Williams, P. T. (2013) Characterization and evaluation of Ni/SiO2 catalysts for hydrogen production and tar reduction from catalytic steam pyrolysis-reforming of refuse derived fuel. *Applied Catalysis B: Environmental*, **134-135**, 238–250.

28. Taeño, M., Maestre, D., Ramírez-Castellanos, J., Li, S., Lee, P. S. and Cremades, A. (2021) Towards Control of the Size, Composition and Surface Area of NiO Nanostructures by Sn Doping. *Nanomaterials*, **11**, 444.

29. Lahuri, A. H., Yarmo Mohd., A. and Tahari, M. N. A. (2021) Ultrasonic Assisted Synthesis of Bimetal Composite Strontium Oxide/Iron(III) Oxide for the Adsorption Isotherm Analysis of CO_2 Capture. *Lecture Notes in Mechanical Engineering*, 175–195.

30. Joachim, J. (2009) Synthesis and Functionalization of Ordered Mesoporous Carbons for Catalytic Applications. *Ph.D. Thesis, Ruhr University Bochum, Germany*.

31. Kantorovich, D., Haviv, L., Vradman, L. and Landau, M. V. (2005) Behaviour of NiO and Nio pohases at high loadings, in SBA-15 and SBA-16 mesoporous silica matrices. Nanoporous Materials IV. *In Proceedings of the 4th International Symposium on Nanoporous Materials*, 147–154.

32. Leyva, C., Rana, M. and Ancheyta, J. (2008) Surface characterization of Al_2O_3-SiO_2 supported NiMo catalysts: An effect of support composition. *Catalysis Today*, **130**, 345–353.

33. Jang, W. -J., Jeong, D. -W., Shim, J. -O., Kim, H. -M., Han, W. -B., Bae, J. W. and Roh, H. -S. (2015) Metal oxide (MgO, CaO, and La_2O_3) promoted Ni-$Ce_{0.8}Zr_{0.2}O_2$ catalysts for H_2 and CO production from two major greenhouse gases. *Renewable Energy*, **79**, 91–95.

34. Naim Ahmad, K., Samidin, S., Salleh, F., Nor Roslam Wan Isahak, W., Al-Amiery, A., Shahbudin Masdar, M., Rahimi Yusop, M., Khalid Al-Azzawi, W., Irwan Rosli, M. and Ambar Yarmo, M. (2022) Carbon Monoxide Desorption and Reduction Studies of Graphitic Carbon Nitride Supported Nickel Catalysts for CO Methanation. *Chemistry Select*, **7**, 1–17.

35. Phuong, P. H., Loc, L. C., Cuong, H. T. and Tri, N. (2018) Effect of NiO Loading and Thermal Treatment Duration on Performance of Ni/SBA-15 Catalyst in Combined Steam and CO_2 Reforming of CH_4. *Materials Transactions*, **59**, 1898–1902.

36. Sieben, J. M., Duarte, M. M. E. and Mayer, C. E. (2010) Electro-Oxidation of Methanol on Pt-Ru Nanostructured Catalysts Electrodeposited onto Electroactivated Carbon Fiber Materials. *ChemCat Chem*, **2**, 182–189.

37. Yang, W., Chu, W., Jiang, C., Wen, J. and Sun, W. (2011) Cerium Oxide Promoted Ni/MgO Catalyst for the Synthesis of Multi-walled Carbon Nanotubes. *Chinese Journal of Catalysis*, **32**, 1323–1328.

38. Zhang, Z., Zhang, X., Zhang, L., Wang, Y., Li, X., Zhang, S., Liu, Q., Wei, T., Gao, G., and Hu, X. (2020) Steam reforming of guaiacol over Ni/SiO_2 catalyst modified with basic oxides: Impacts of alkalinity on properties of coke. *Energy Conversion and Management*, **205**, 112301.

39. Sricharoenchaikul, V., Atong, D., Sornkade, P., and Nisamaneenate, J. (2017) Performance of Ni/dolomite pellet catalyst on gas distribution from cassava rhizome gasification with a modular fixed-bed gasifier. *Environmental Technology*, **38**, 1176–1183.

40. Zhang, H., Li, M., Xiao, P., Liu, D. and Zou, C. J. (2013) Structure and Catalytic Performance of Mg-SBA-15-Supported Nickel Catalysts for CO_2 Reforming of Methane to Syngas. *Chemical Engineering & Technology*, **36**, 1701–1707.

41. Li, D., Zeng, L., Li, X., Wang, X., Ma, H., Assabumrungrat, S. and Gong, J. (2015) Ceria-promoted Ni/SBA-15 catalysts for ethanol steam reforming with enhanced activity and resistance to deactivation. *Applied Catalysis B: Environmental*, **176-177**, 532–541.

42. Hasnan, N. S. N., Timmiati, S. N., Pudukudy, M., Yaakob, Z., Lim, K. L. and Taufiq-Yap, Y. H. (2019) Catalytic decomposition of methane into hydrogen and carbon nanotubes over mesostructured silica nanoparticle-supported nickel catalysts. *Journal of Porous Materials*, **27**, 369–382.